Implementation of Fuchs' model of ion diffusion charging of nanoparticles considering the electron contribution in dc-corona chargers in high charge densities

2009 J. Phys. D: Appl. Phys. 42 125206

(http://iopscience.iop.org/0022-3727/42/12/125206)

IOP PUBLISHING JOURNAL OF PHYSICS D: APPLIED PHYSICS

J. Phys. D: Appl. Phys. **42** (2009) 125206 (10pp) doi:10.1088/0022-3727/42/12/125206

Implementation of Fuchs' model of ion diffusion charging of nanoparticles considering the electron contribution in dc-corona chargers in high charge densities

A Aliat[1,2], C T Hung[1], C J Tsai[2] and J S Wu[1,3]

[1] Department of Mechanical Engineering, National Chiao Tung University, Hsinchu 30050, Taiwan
[2] Institute of Environmental Engineering, National Chiao Tung University, Hsinchu 30050, Taiwan

E-mail: chongsin@faculty.nctu.edu.tw

Received 10 January 2009, in final form 1 May 2009
Published 1 June 2009
Online at stacks.iop.org/JPhysD/42/125206

Abstract

A 1D corona discharge model coupled to a 2D-axisymmetric particle charging model are proposed in this paper to simulate nanoparticle charging process within a wire-tube air corona discharge subjected to an applied positive or negative dc voltage. This 1D discharge model provides the distribution of the electric field, the air ion and free electron concentrations for the 2D charging model which in turn solves the spatial distributions of the various charged nanoparticles within the tube. This 2D charging model takes into account the effect of electrons, on the basis of Fuchs' law usually employed in the literature for modelling of ion diffusion nanoparticle charging. The current approach is valid when the concentration of nanoparticles is much lower than the concentration of ionic species in the gas. Numerical results show that the positive air ions can be assumed to be solely responsible for the charging process in a positive air corona charger, while both the negative air ions and electrons play an important role in the negative charging. At high negative charge intensities, the effect of the electrons becomes appreciable due to their high conduction velocity. In general, the numerical results obtained are in good agreement with the experimental data reported in the literature.

(Some figures in this article are in colour only in the electronic version)

1. Introduction

Nanoparticle charging plays an important role in both scientific studies and practical applications related to aerosols, especially for those in the nanometre range i.e. <100 nm. Charging of nanoparticles has been applied in a number of different areas, such as material synthesis, nano-structure patterning, contamination control and particle instrumentation [1]. Diffusion-based charging is by far the most commonly used technique for charging the nanoparticles. In this process, the nanoparticles are exposed for a certain period of time to an ionized gas environment normally generated by air corona discharges. The diffusion theory based on Fuchs' law [2] is known to be used to model the charging mechanisms of nanoparticles, and has been experimentally verified in positive air corona chargers [3, 4]. This diffusion theory was also used in a negative air corona charger as shown by the work of Marquard *et al* [5]. However, these authors have found that Fuchs' diffusion theory fails to properly model the charging mechanisms at high charging intensities, i.e. at high Nt-product (N corresponds to the mean concentration of the air ions, whereas t is the mean time residence of the nanoparticles within the corona charger). Indeed, the measured average charges carried by the nanoparticles (with diameter of 65 nm) are considerably larger than the predicted

[3] Author to whom any correspondence should be addressed.

values up to 1.6 times, in which the reason could not be explained.

Until very recently, we have briefly presented a 2D theoretical charging model [6] that predicts the path of nanoparticles within the wire-tube, which is crucial in optimizing the design and hence the charging effectiveness of device chargers. This charging model demonstrated that Fuchs' law considered only air ions in the diffusion theory, and that free electrons must be taken into account to explain the above large discrepancy between the predicted and the experimental data. Indeed, probably Fuchs did not deal with the electron contribution because it requires a high dc field which leads to a poor extrinsic charge efficiency (= fraction of charged nanoparticles leaving the corona charger) due to the electron collection within the corona charger.

However, the charging model in [6] was only briefly presented and was applied with only one experimental condition of Marquard *et al* [5], i.e. for an air gas carrier's velocity of 2 m s^{-1} and a negative cylindrical direct current (dc) air corona with a length of 26 cm and a radius of 2 cm in radius. It is thus the objective of this paper to present the details of this model and its validity with other experimental data Marquard *et al* [5]. As far as we know, only these authors provide experimental data in high charging intensities. The theoretical charging model [6] definitely requires to be confirmed with other sizes than nanoparticles with a diameter of 65 nm in the future.

In this paper, we present in detail the charging model [6] which consists of a 1D corona discharge model and a 2D-axisymmetric nanoparticle charging model. Applications with various velocities of the air gas carrier, both positive and negative charging cases, are taken into account by considering a smaller wire-tube in length (6 cm). The numerical results obtained will be discussed by comparing with the experimental data of Marquard *et al* [5], and finally the important findings of this study are summarized at the end of this paper.

2. Corona discharge model

Some physical models in dc-corona discharge have been developed and can be found in [7–11]. The wire-tube corona device utilized by Marquard *et al* [5] is illustrated in figure 1. It is a metal tube with length $L = 6$ cm and inner radius $R = 2$ cm filled with flowing dry air, in which a tungsten wire is stretched along the axis. The tungsten wire electrode with a radius of $r_w = 0.05$ mm is subjected to a positive or a negative dc voltage ϕ_w with the current intensity per unit of length I. The applied electrical potential ϕ_w is assumed to be high enough to sustain a corona regime in a stationary state [12]. The outer electrode which is made of stainless steel tube is grounded. We assume inside the wire-tube charger that the air is at atmospheric pressure and at uniform room temperature.

Uncharged nanoparticles at the entrance of the tube are carried into the corona charger by the flowing dry air. The air corona discharge leads to the formation of free electrons, positive and negative air ions [13]. These charged species are characterized by their number concentration N_e, N_+, N_- and

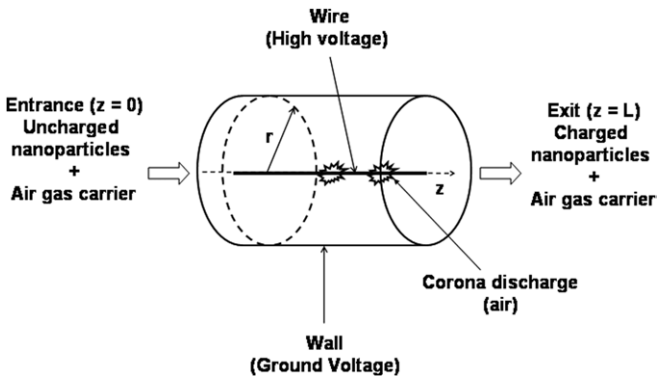

Figure 1. Sketch of direct current (dc) corona charger with wire-tube configuration.

their electrical mobility coefficients μ_e, μ_+, μ_-, respectively. Their presence within the wire-tube leads to the formation of charged nanoparticles at the exit of the wire-tube charger.

By neglecting the electric wind [14], the stationary corona discharge is governed by the time-independent continuity equations for each charged species i (electrons, positive and negative air ions) [15]:

$$\nabla \cdot \vec{J}_i = S_i, \tag{1}$$

where S_i is the production term, and the flux of the charged species i is given by

$$\vec{J}_i = \frac{e_i}{e_0} N_i \mu_i \vec{E}. \tag{2}$$

where e_i is the charge carried by the species i and e_0 the absolute value of the electron charge. The local electric field strength $\vec{E}$ is governed by the Maxwell–Gauss equation:

$$\nabla \cdot \vec{E} = \frac{1}{\varepsilon_0} \sum_i e_i N_i, \tag{3}$$

where $\varepsilon_0$is the permittivity of free space. Note that the flux of charged species (2) only consists of the drift conduction term due to the electric field by ignoring the diffusion conduction term [16]. Since the corona discharge is assumed to be axisymmetric and invariant in the axial direction, the stationary continuity equations (1) can be simplified as one-dimensional form and rewritten as follows:

$$\frac{1}{r}\frac{\mathrm{d}}{\mathrm{d}r}\left(r\frac{e_i}{e_0}N_i\mu_i E\right) = S_i, \tag{4}$$

where r is the radial coordinate, i.e. the distance to the centre of the wire. The above production term S_i of electrons, positive and negative air ions are given by [16]

$$S_e = \mp(\alpha - \eta)\, N_e \mu_e E, \tag{5}$$

$$S_+ = \pm\alpha N_e \mu_e E \tag{6}$$

and

$$S_- = \mp\eta N_e \mu_e E. \tag{7}$$

The sign in equations (5) and (7) is negative if the active electrode (wire) is subjected to a positive potential and positive

vice versa. In contrast, the sign in equation (6) is positive if the wire electrode is subjected to a positive potential and negative vice versa. Mean values of spectral distributions of electrical mobilities are $\mu_+ = 1.4 \times 10^{-4}$ and $\mu_- = 1.9 \times 10^{-4}\,\mathrm{cm^2\,V^{-1}\,s^{-1}}$ [4] related to the positive and negative air ions, respectively. However, the electrical mobility of electrons μ_e, the ionization coefficient α and the attachment coefficient η all depend upon the local electric field E and are given in the appendix.

The Deutsch assumption [17], which stipulates that the space charge affects only the magnitude of the electric field but not its direction, is satisfied in coaxial cylindrical configurations [18]. In the current study, the air ion concentration ($\sim 10^9\,\mathrm{cm^{-3}}$) is much larger than that of nanoparticles ($\sim 10^5\,\mathrm{cm^{-3}}$) and electrons (~2–3 orders of magnitude smaller than air ions). The space charge between electrodes thus essentially originates from the air ions, which leads to the following simplified Gauss equation, based on the symmetry of the discharge [15]:

$$\frac{1}{r}\frac{\mathrm{d}}{\mathrm{d}r}(rE) = \frac{I}{2\pi r \mu \varepsilon_0 E}. \tag{8}$$

Rigorously speaking, the above equation is only valid in the region where the current intensity is carried almost exclusively by one kind of charged species characterized by its electrical mobility μ [15]. We will see later that for a positive (negative) corona the current intensity is almost carried by the positive (negative) air ions so that we can simply put $\mu = \mu_+$ ($\mu = \mu_-$) in equation (8). In addition, by Kaptsov's assumption [19], which considers that the electric field on the corona wire's surface remains constant at the value resulting from Peek's formula [20] defined as

$$E_\mathrm{w} = E(r = r_\mathrm{w}) = 30\delta\left[1 + \frac{0.3}{(\delta r_\mathrm{w})^{1/2}}\right], \tag{9}$$

where E_w is in $\mathrm{kV\,cm^{-1}}$ and the wire's radius r_w in cm; $\delta (= T_0 P / T P_0)$ is the relative density of the air gas, in which $T_0 (= 298\,\mathrm{K})$ and $P_0 (= 1\,\mathrm{atm})$ are the reference temperature and pressure, respectively. The assumption that the electric field strength at the wire's surface is equal to Peek's onset field is generally acceptable in particle charging modelling and has been demonstrated in detail by Morrow [21]. By utilizing equation (9) as the boundary condition of equation (8), the expression of the local electric field can be expressed as follows:

$$E(r) = \left[\left(\frac{I}{\varepsilon_0 2\pi\mu_\pm}\right) \times \left(1 - \frac{r_\mathrm{w}^2}{r^2}\right) + \left(\frac{E_\mathrm{w} r_\mathrm{w}}{r}\right)^2\right]^{1/2} \tag{10}$$

in which the air ion electrical mobility depends on whether the discharge is positive ($\mu = \mu_+$) and negative ($\mu = \mu_-$).

Because of the Coulomb repulsion of charged species on the electrodes, boundary conditions of the air ion continuity equations (4) are $N_+(r = r_\mathrm{w}) = 0$ and $N_-(r = R) = 0$ for a corona subjected to a positive high voltage. Similarly, for a negative discharge these boundary conditions become $N_-(r = r_\mathrm{w}) = 0$ and $N_+(r = R) = 0$. As for the continuity equation of electrons, its boundary condition on the wire's surface is given by the current intensity determined experimentally [22]:

$$I = 2\pi r_\mathrm{w}\left(\sum_i |e_i|\mu_i N_i E\right)_{r_\mathrm{w}}, \tag{11}$$

where only the electrons and positive (negative) air ions have a non-zero contribution to the current intensity for a positive (negative) discharge.

All the above equations are discretized by the central finite-difference method and are then solved using an iterative algorithm for the matrix equations.

For a positive (negative) corona, the diffusion theory considers that only positive (negative) air ions are responsible for the charging of nanoparticles. In this condition, the current density is assumed to be carried exclusively by these air ions and their concentration is given by utilizing equations (10) and (11):

$$N_\pm(r) = \frac{I}{2\pi e_0 \mu_\pm}\left[\left(\frac{I}{\varepsilon_0 2\pi\mu_\pm}\right)\left(1 - \frac{r_\mathrm{w}^2}{r^2}\right) + \left(\frac{E_\mathrm{w} r_\mathrm{w}}{r}\right)^2\right]^{-1/2}. \tag{12}$$

Figure 2 illustrates the distributions of the charged species as a function of the radial position in the region very close to the powered wire within a positive air corona discharge. These results were obtained for a voltage of $\phi_\mathrm{w} = +9.8\,\mathrm{kV}$ and $I = 16.7\,\mu\mathrm{A\,cm^{-1}}$, which corresponds to one of the experimental data of Marquard *et al* [5]. These distributions are obtained by solving the continuity equations (4) for the electrons, the positive and negative air ions. In the detailed model, the density of positive air ions is at least four orders of magnitude higher than the densities of electrons and negative air ions, which shows that the negative air ions and electrons may be neglected in practice. These trends are similar to the

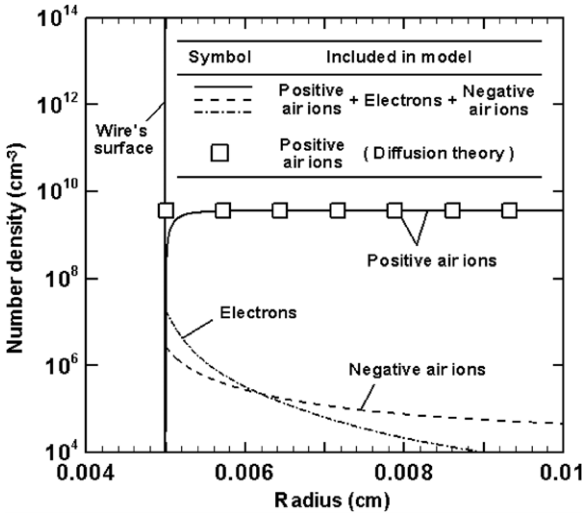

Figure 2. Distribution of the electrons, positive and negative air ions. The wire-tube corona is 2 cm radius and submitted at $\phi_\mathrm{w} = +9.8\,\mathrm{kV}$ with $I = 16.7\,\mu\mathrm{A\,cm^{-1}}$.

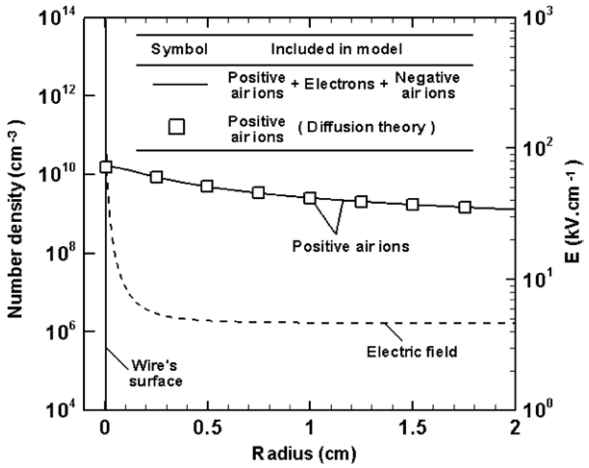

Figure 3. Distribution of the positive air ions and the electric field. The wire-tube corona is 2 cm in radius and submitted at $\phi_w = +9.8\,\text{kV}$ with $I = 16.7\,\mu\text{A cm}^{-1}$.

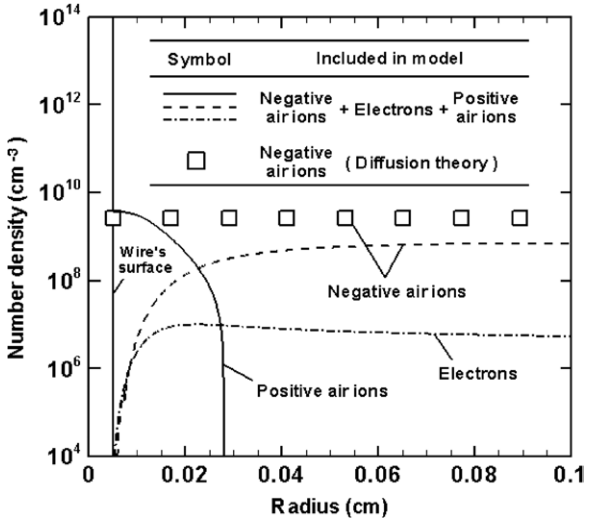

Figure 4. Distribution of the electrons, positive and negative air ions. The wire-tube corona is 2 cm in radius and submitted at $\phi_w = -8.8\,\text{kV}$ with $I = 16.7\,\mu\text{A cm}^{-1}$.

results obtained by Chen and Davidson [13] and Takahashi *et al* [23]. Moreover, the concentration of the positive air ions predicted by the detailed model coincides very well with that by equation (12) based on the diffusion theory starting at the distance of 0.001 cm from the wire's surface. Large deviation can still be found near the wire surface, i.e. in the ionization region. Similar to the diffusion theory, the positive charging is solely caused by the positive air ions. Indeed, as shown in figure 3 the current is essentially carried by these positive air ions in the drift region ($\geqslant$0.001 cm from the wire's surface which occupies almost the entire volume of the wire-tube charger.

In contrast, figure 4 shows the distributions of the charged species within a negative air corona very close to the powered wire, in which the potential is $\phi_w = -8.8\,\text{kV}$ with the same current per length in the case of positive corona [5]. Based on the detailed model, the ionization region where the positive air ions are dominant is found to be much larger ($\sim$0.025 cm from the wire's surface) as compared with that of the positive

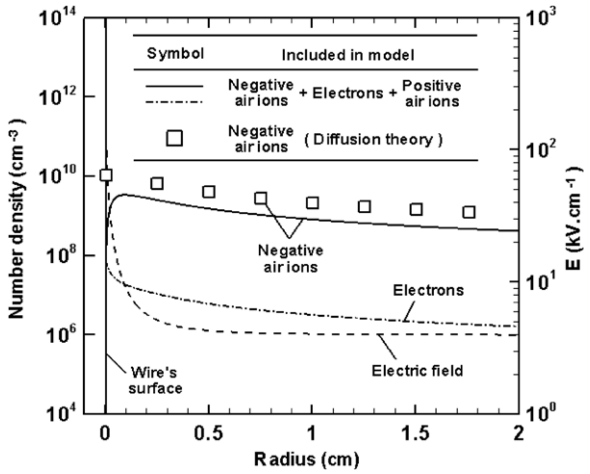

Figure 5. Distribution of the negative air ions and the electric field. The wire-tube corona is 2 cm in radius and submitted at $\phi_w = -8.8\,\text{kV}$ with $I = 16.7\,\mu\text{A cm}^{-1}$.

corona. In addition, the concentration of negative air ions is lower than that predicted using equation (12) because the current flux is not only carried by the negative air ions but also the electrons in the drift region (see figure 5). Nevertheless, the positive air ions can also be neglected in the negative charging model, because the drift region occupies the major portion of the wire-tube charger. The concentration of electrons is about two orders of magnitude smaller than the negative air ions, which is appreciable as compared with the case of the positive air corona. Despite their low concentration the electrons have been shown to play an important role in the negative charging of nanoparticles at high *Nt*-product and thus cannot be neglected [6]. This is because of the much larger electrical mobility of the electrons as compared with the air ions. It is noted that in figures 3 and 5 the values for the electrical mobility of electrons in the ionization and drift regions are calculated to be $\mu_e \sim 300$ and $\sim$820 $\text{cm}^2\,\text{V}^{-1}\,\text{s}^{-1}$, respectively, based on the formula in the appendix. Indeed, when the local field becomes higher, the electron temperature is raised, the rate of collision increases and the electrical mobility decreases, as described in [24].

Figure 6 shows the evolution of the same variables than figure 5, in which the potential is $\phi_w = -5.2\,\text{kV}$ with the current per length of $I = 0.33\,\mu\text{A cm}^{-1}$ [5]. The concentrations of negative air ions and electrons are found to be about two orders of magnitude lower than in figure 5.

We have observed that the ionization region only occupies a negligible portion of the corona charger for both positive and negative cases. The current flux which is essentially carried by the air ions (either positive or negative alone) in the drift region leads to a fairly good approximation of the electric field based on equation (10). Figures 3 and 5 show that the electric field decreases rapidly with increasing radial position and becomes nearly constant after $r = 0.5\,\text{cm}$. However, the rate of decrease in the electric field with respect to the radial distance is slower for the lower current density case (see figure 7). As the electric field is not considered to be constant in this study, the charging model presented in this paper predicts more precisely the average charges carried by the nanoparticles.

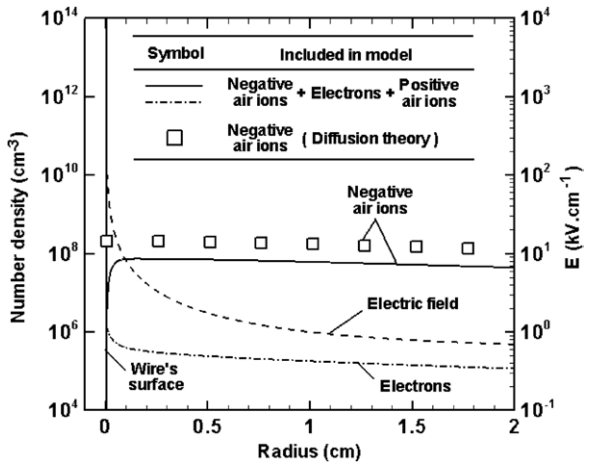

Figure 6. Distribution of the negative air ions and the electric field. The wire-tube corona is 2 cm in radius and submitted at $\phi_w = -5.2\,\text{kV}$ with $I = 0.33\,\mu\text{A cm}^{-1}$.

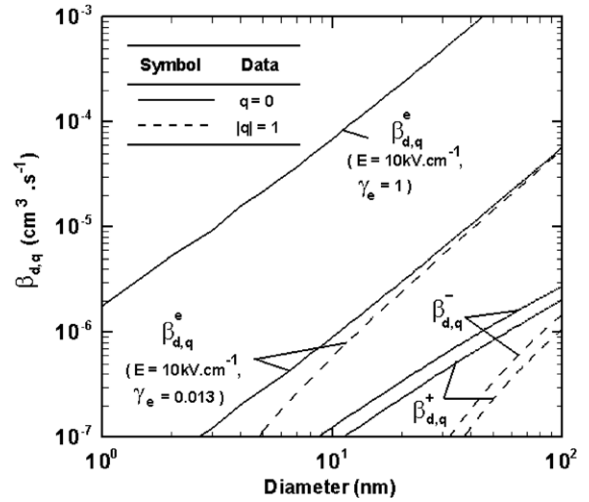

Figure 7. Predicted attachment rate coefficients $\beta_{d,q}$ of electrons ($\gamma_e = 1$ and 0.013), positive and negative air ions to uncharged ($q = 0$) and charged ($|q| = 1$) nanoparticles.

3. Nanoparticle charging model

Several works related to nanoparticle charging and kinematics in dc corona can be found in [7, 25–30]. In this study, the distribution of nanoparticles within the charger device is governed by the following time-independent continuity equations:

$$\nabla \cdot \vec{J}_{d,q} = S_{d,q}, \tag{13}$$

where $\vec{J}_{d,q}$ and $S_{d,q}$ are the flux and the production term related to the spherical nanoparticles of diameter d with q elementary charges, respectively. The transport of nanoparticles is a combination of several factors which include convection due to carrier air flow, drift due to the electric field and diffusion due to the concentration gradient. The current density can thus be written as follows:

$$\vec{J}_{d,q} = N_{d,q}\vec{U} + N_{d,q}\, q\, \mu_d \vec{E} - D_d \nabla . N_{d,q}, \tag{14}$$

where the vector $\vec{U}$ describes the mean carrier air flow velocity. Terms $N_{d,q}$ and μ_d are the number density and the coefficient of electrical mobility of nanoparticles, respectively.

The distribution of nanoparticles within the wire-tube charger is assumed to be axisymmetric. Moreover, a typical velocity profile of the fully-developed turbulent pipe flow [31] is adopted based on the experimental conditions of Marquard *et al* [4]. With these conditions, the continuity equation (13) can be rewritten as:

$$U_z \frac{\partial N_{d,q}}{\partial z} + |q|\,\mu_d E \frac{\partial N_{d,q}}{\partial r} + |q|\,\mu_d N_{d,q}\left(\frac{E}{r} + \frac{\partial E}{\partial r}\right) - D_d\left(\frac{1}{r}\frac{\partial N_{d,q}}{\partial r} + \frac{\partial^2 N_{d,q}}{\partial r^2} + \frac{\partial^2 N_{d,q}}{\partial z^2}\right) = S_{d,q} \tag{15}$$

in which we applied the following boundary conditions to solve them:

- at the entrance of the wire-tube charger, $N_{d,q=0}(z = 0) = N_0$ and $N_{d,q\neq 0}(z = 0) = 0$ where N_0 is the initial concentration of uncharged nanoparticles;
- at the exit of the tube, the wire's surface and grounded electrode, $\partial N_{d,q}/\partial \vec{n} = 0$ ($\vec{n}$ is the normal unit vector on the considered surface). The nanoparticles do not undergo any physical processes at the exit, and catalytic processes on the tube surfaces are neglected.

The general production term of nanoparticles in the continuity equations (15) can be written as

$$S_{d,q} = \beta^{+}_{d,q-1} N_{+} N_{d,q-1} - \beta^{+}_{d,q} N_{+} N_{d,q} + \beta^{-}_{d,q+1} N_{-} N_{d,q+1} - \beta^{-}_{d,q} N_{-} N_{d,q} + \beta^{e}_{d,q+1} N_{e} N_{d,q+1} - \beta^{e}_{d,q} N_{e} N_{d,q}, \tag{16}$$

where the first term on the right-hand side describes the generation rate of nanoparticles of diameter d with q elementary charges by the attachment between a positive air ion and a nanoparticle with $q - 1$ elementary charges. The third (fifth) term on the right-hand side describes the rate of generation by the attachment between a negative air ion (electron) and a nanoparticle with $q + 1$ elementary charges. The second, fourth and the sixth terms on the right-hand side indicates the loss rate of the nanoparticles of diameter d with q elementary charges by their attachment with a positive air ion, a negative air ion and an electron, respectively. The attachment rate coefficients of positive air ions $\beta^{+}_{d,q}$, of negative air ions $\beta^{-}_{d,q}$ and of electrons $\beta^{e}_{d,q}$ to nanoparticles are given in the appendix at the end of this paper. The latter is characterized by a probability γ_e that an electron is captured by a nanoparticle inside its limiting-sphere. A value of $\gamma_e = 0.013$ is used in [6] for nanoparticles with diameter of 65 nm for some specific flow conditions. It was suggested that this low value results from the high conduction velocity of electrons ($v_e = \mu_e E$). Indeed, with appreciable amount of electrons in the drift region of a negative air corona, the electrons play an important role in nanoparticle charging due to the higher electrons flux ($= N_e v_e$) moving through the limiting sphere. As we consider the same size of nanoparticles, we applied the above value of capturing probability for the electrons in this study. Note that for the attachment rate coefficient of air ions $\beta^{\pm}_{d,q}$, the probability that an air ion is captured by a nanoparticle inside its limiting-sphere is usually assumed to be equal to the unity ($\gamma^{\pm} = 1$).

Figure 7 illustrates the effects of nanoparticle size on the attachment rate coefficients $\beta_{d,q}$ of the electron, the positive

and negative air ions onto the uncharged ($q = 0$) and charged ($|q| = 1$) nanoparticle with the applied electric field of $10\,\mathrm{kV\,cm^{-1}}$. Note that only the attachment rate coefficient of electrons strongly depends on the electric field because of its dependence on the electrical mobility μ_e and the diffusion coefficient D_e of electrons. As expected, all the attachment coefficients increase with increasing size of the nanoparticles. For a capturing probability equal to unity for all the charged species, the attachment rate coefficient $\beta^{e}_{d,q=0}$ related to the electrons is about three orders of magnitude higher than the ionic rate coefficients $\beta^{\pm}_{d,q=0}$. This observation is due to the high conduction velocity of electrons v_e as explained earlier. Similarly, the attachment coefficients of negative air ions are higher than those of positive air ions simply because of larger conduction velocity due to higher mobility of negative air ions. As expected the values of attachment rate coefficient of electrons become smaller when the probability of capture γ_e decreases.

Figure 7 also shows that the attachment coefficients of all charged species onto a nanoparticle with $|q| > 0$ elementary charges decrease with increasing number of charges. However, the electron attachment coefficients become close to each other at higher diameter of the nanoparticles, which is especially true for the present test case ($d = 65\,\mathrm{nm}$). Moreover, the nanoparticles are unlikely to be highly charged if the size becomes very small which is in line with observations of Pui *et al* [3] and Alguacil and Alonso [30]. Indeed, these studies showed that charging efficiency of nanoparticles decreases experimentally with decreasing diameter. However, the attachment process between an electron and a charged nanoparticle remains relatively efficient, because of the great conduction velocity of electrons as compared with that of ions. Indeed, this large velocity leads to a stronger flux of electrons moving through the limiting-sphere of nanoparticles.

4. Comparison with experiments

Figure 8 illustrates the average charge carried by the nanoparticles at the exit of the positive (negative) corona charger as a function of the Nt-product. The numerical results are obtained by considering only the positive (negative) air ions by using equation (12) in the case of a positive (negative) discharge. We can see that these results are in good agreement with the ion diffusion Fuchs' model by considering only positive air ions, which is known to reproduce the experimental measurements in the case of positive charging [3, 4]. This finding validates the 2D-axisymmetric charging model employed in the current study. The average charge carried by the nanoparticles is greater in negative discharge because attachment coefficients of the negative air ions are higher than those of the positive air ions (see figure 7). However, the diffusion theory by considering only negative air ions and based on Fuchs' law fails to predict accurately the negative nanoparticle charging in particular at high charging intensities, which is shown next.

In contrast, figure 9 illustrates the average charge carried by the nanoparticles at the exit of the negative corona charger as a function of the Nt-product. It is clear that the diffusion

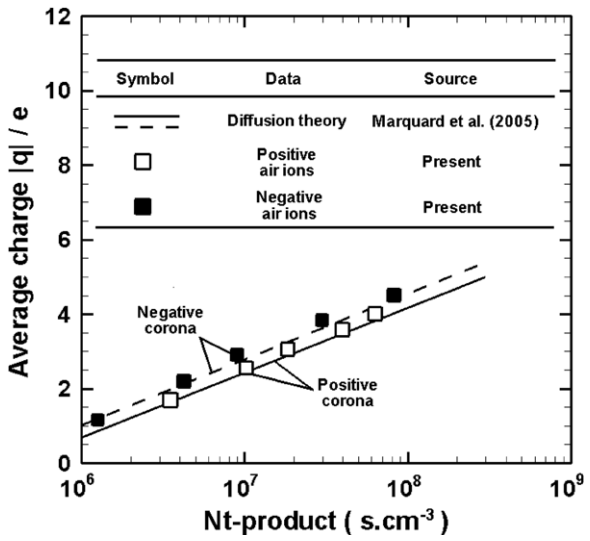

Figure 8. Predicted average charge carried by the nanoparticles with diameter of 65 nm by considering only air ions as a function of the Nt-product. The wire-tube corona is 6 cm in length and 2 cm in radius. The mean velocity of the carrier gas is $2\,\mathrm{m\,s^{-1}}$.

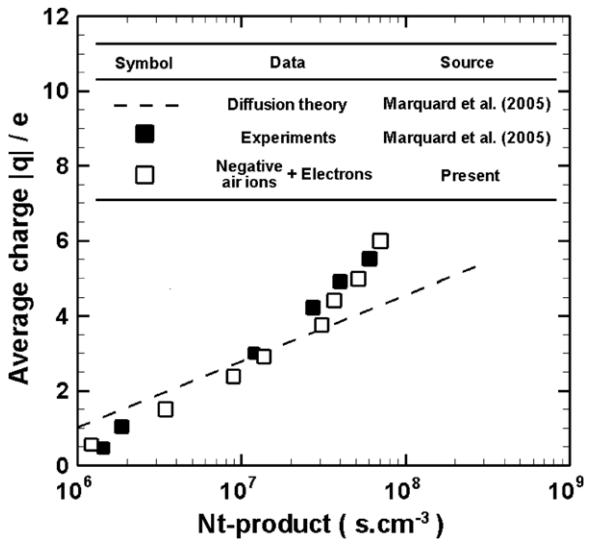

Figure 9. Evolution of the average charge carried by the nanoparticles with diameter of 65 nm within a negative corona discharge as a function of the Nt-product. The wire-tube corona is 6 cm in length and 2 cm in radius. The mean velocity of the carrier gas is $2\,\mathrm{m\,s^{-1}}$.

theory which considers only the attachment of negative air ions fails to predict the average charge at the exit of the charger. Interestingly, the present complete 2D charging model, based on Fuchs' model, which takes into account the effect of electrons and negative air ions agrees very well with the measurements. Although the concentration of electrons is much lower than that of negative air ions (see figure 5, which corresponds to $Nt \sim 5 \times 10^7\,\mathrm{s\,cm^{-3}}$), their attachment coefficients are very high as compared with that of negative air ions. At low Nt-product the average charges predicted by the diffusion theory are higher than the measurements because it does not take into account the electrons. Indeed, the charging process is essentially caused by the negative air ions at low

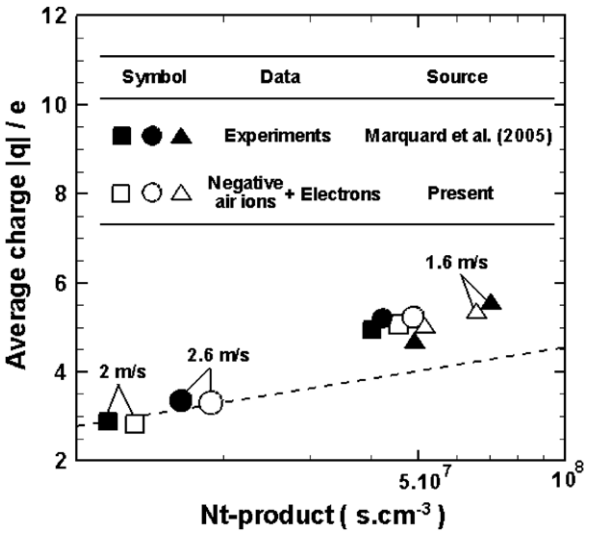

Figure 10. Evolution of the average charge carried by the nanoparticles with diameter of 65 nm within a negative corona discharge with various mean air gas carrier's velocity as a function of the Nt-product. The wire-tube corona is 6 cm in length and 2 cm in radius.

Nt-product (the concentration of electrons is too low) and the diffusion theory considers the current is carried only by these air ions, which leads to a higher ionic concentration (see figure 6, which corresponds to $Nt \sim 3.5 \times 10^6\,\mathrm{s\,cm^{-3}}$). Finally, a low value of the capturing probability of electrons ($\gamma_e = 0.013$) leads to satisfactory numerical results as compared with the measurements.

Figure 10 illustrates the comparison of the prediction by the complete negative charging model with the measurements at various flow velocities (1.6, 2 and 2.5 m s^{-1}) using the same capturing probability of electron ($\gamma_e = 0.013$). It is clear that the numerical results obtained by the 2D model are in good agreement with the experimental data of Marquard *et al* [5]. This shows that this low capturing probability of electron is insensitive, at least, to the above simulation conditions.

Figure 11 shows the distribution of the nanoparticles with $q = 0, -1, -2, -3, -4, -5, -6, -8$ and -10 elementary charges within the negative wire-tube charger illustrated by figure 5 ($\phi_w = -8.8\,\mathrm{kV}$, $I = 16.7\,\mu\mathrm{A\,cm^{-1}}$) with a carrier gas mean velocity of 2 m s^{-1}, which corresponds to $Nt \sim 5 \times 10^7\,\mathrm{s\,cm^{-3}}$. The nanoparticles acquire quickly electrical charge near the wire, because of the high concentration of the attachment partners (electrons and negative air ions) near the wire's surface, as shown in figure 5. Charged particles are then carried by the dry air flow further downstream and at the same time move towards the outer electrode wall due to radial electric field. This can be confirmed from the location of peak value of concentration of various elementary charges. For higher charges, say, $q = -10$, there is not enough time and space for the nanoparticles to be charged. Thus, its concentration is very low as compared with those of lower charges such as $q = -4$ and $q = -5$, which leads to an average charge of $\bar{q} \sim 4.8$ at $Nt \sim 5 \times 10^7\,\mathrm{s\,cm^{-3}}$ at the exit of the wire-tube, as shown in figures 9 and 10.

Figure 12 illustrates the same distributions and air gas carrier's velocity within a positive corona discharge shown

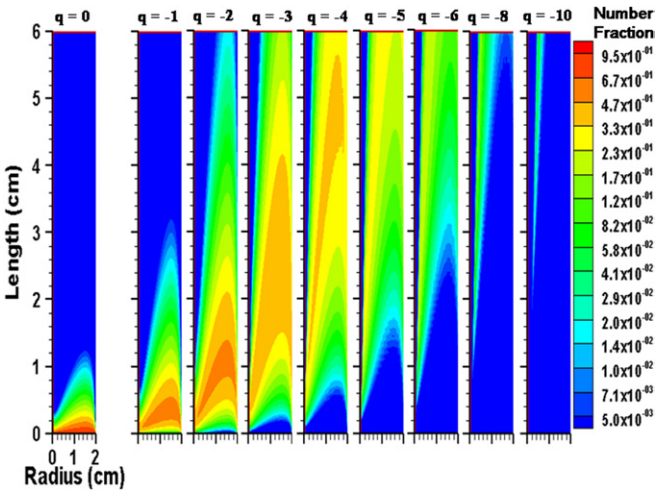

Figure 11. Distribution of the nanoparticles with diameter of 65 nm. The wire-tube corona is 6 cm in length and 2 cm in radius and submitted at $\phi_w = -8.8\,\mathrm{kV}$ with $I = 16.7\,\mu\mathrm{A\,cm^{-1}}$. The mean velocity of the carrier gas is 2 m s^{-1}.

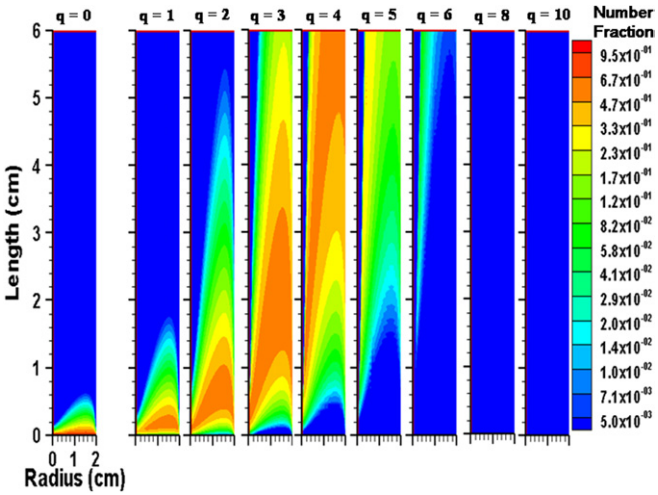

Figure 12. Distribution of the nanoparticles with diameter of 65 nm. The wire-tube corona is 6 cm in length and 2 cm in radius and submitted at $\phi_w = +9.8\,\mathrm{kV}$ with $I = 16.7\,\mu\mathrm{A\,cm^{-1}}$. The mean velocity of the carrier gas is 2 m s^{-1}.

in figure 3 ($\phi_w = 9.8\,\mathrm{kV}$, $I = 16.7\,\mu\mathrm{A\,cm^{-1}}$). Their behaviour is the same as in the case of negative corona. However, the positive wire-tube charger is inefficient in charging nanoparticles as compared with negative one because only the positive air ions are responsible of the charging process. Indeed, we have seen previously that the attachment rate coefficients related to the positive air ions are much lower than those of negative air ions and electrons present in the negative corona discharge. Thus, with the same current intensity most of the nanoparticles carry $q = 4$ elementary charges at the exit of the wire-tube. This leads to an average charge $\bar{q} \sim 4$ at $Nt \sim 6 \times 10^7\,\mathrm{s\,cm^{-3}}$, which is lower than that of the negative charger.

Figure 13 shows the average charge carried by the nanoparticles as a function of their mean residence time within the wire-tube, in which the potential is $\phi_w = -8.8\,\mathrm{kV}$ with the current per length of $I = 16.7\,\mu\mathrm{A\,cm^{-1}}$. This figure shows

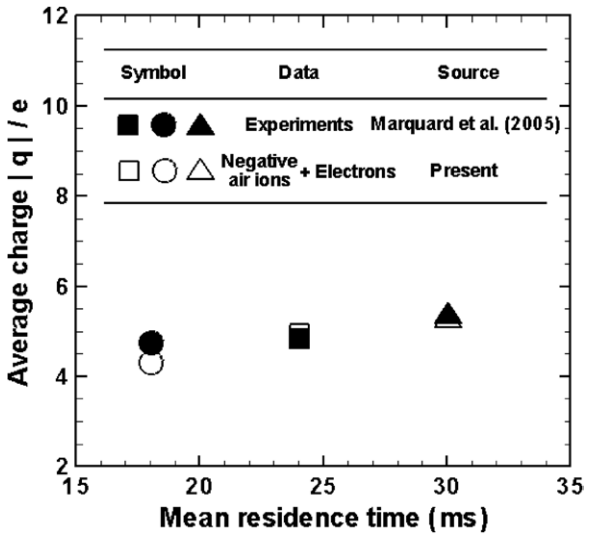

Figure 13. Evolution of the average charge carried by the nanoparticles with diameter of 65 nm within a negative corona discharge as a function of the mean residence time. The wire-tube corona is 6 cm in length and 2 cm in radius and submitted at $\phi_w = -8.8$ kV with $I = 16.7\,\mu$A cm^{-1}.

that nanoparticles are even more charged as they stay with longer time in the charger device. However, this may not be true if longer tube or higher electric field is considered [6], which is beyond the scope of the current study.

5. Conclusion

A 1D corona discharge model and a 2D-axisymmetric nanoparticle charging model are proposed in this paper to simulate nanoparticle charging within a wire-tube air corona ionizer subjected to positive or negative voltage. This approach is valid provided that the concentration of nanoparticles is much lower than the concentration of charged species in the gas. The numerical results obtained with an air corona discharge and nanoparticles with diameter of 65 nm are in good agreement with the experimental data. The ionization region of the corona discharge can be neglected in charging process. Only positive air ions are considered in positive charging and the results of the 2D charging model are consistent with the ion diffusion theory. However, the free electrons must be taken into account (with capturing probability $\gamma_e = 0.013$) together with the negative air ions in the negative charging. With the same current, the charging efficiency of a negative corona charger outperforms greatly that of a positive corona charger. Charged species (electrons) with high conduction velocity play an important role on the nanoparticle charging mechanisms. More measurements using nanoparticles with different sizes and number concentrations are strongly recommended to further test the validity of the 2D charging model presented in the study.

Acknowledgments

The financial support of the National Science Council of Taiwan through the contracts NSC-96-2628-E-009-008-MY3, NSC-96-2120-M-006-005 and NSC-96-2628-E-009-134-MY3 is gratefully acknowledged.

Appendix

Ionization rate coefficient of gas molecules. The ionization coefficient $\alpha(\text{cm}^{-1})$ is expressed as [32, 33]

$$\alpha/P = \exp[\text{Pol}(E/P)], \tag{A.1}$$

where $E/P \geqslant 35\,\text{V cm}^{-1}\,\text{Torr}^{-1}$, and $\text{Pol}(E/P)$ is a polynomial whose coefficients are given by

$$a_0 = -0.64927 \times 10^2, \quad a_1 = 0.52642 \times 10^1,$$
$$a_2 = -0.20238 \times 10^0, \quad a_3 = 0.45178 \times 10^{-2},$$
$$a_4 = -0.63081 \times 10^{-4}, \quad a_5 = 0.56724 \times 10^{-6},$$
$$a_6 = -0.32780 \times 10^{-8}, \quad a_7 = 0.11739 \times 10^{-10},$$
$$a_8 = -0.23661 \times 10^{-13}, \quad a_9 = 0.20479 \times 10^{-16},$$

P is the pressure in Torr and $E$is the electric field in V cm^{-1}.

Attachment rate coefficient of electrons to gas molecules. The attachment coefficient $\eta(\text{cm}^{-1})$ is expressed as [32, 33]

$$\eta/P = 1.95\exp(-60P/E)/(E/P), \tag{A.2}$$

where P is the pressure in Torr and E is the electric field in V cm^{-1}.

Electrical mobility of electrons. The electrical mobility $\mu_e(\text{cm}^2\,\text{s}^{-1}\,\text{V}^{-1})$ is the electron velocity coefficient (v_e) divided by the local electric field E. The electron velocity $v_e(\text{cm s}^{-1})$ was expressed as [32, 33]

$$v_e = 100 \times 10^4 (E/P)^{0.715}$$
$$\text{for } E/P \leqslant 100\,\text{V cm}^{-1}\,\text{Torr}^{-1},$$
$$v_e = 155 \times 10^4 (E/P)^{0.62}$$
$$\text{for } E/P > 100\,\text{V cm}^{-1}\,\text{Torr}^{-1},$$

where P is the pressure in Torr and E is the electric field in V cm^{-1}.

Diffusion coefficient of electrons. The diffusion coefficient $D_e(\text{cm}^2\,\text{s}^{-1})$ is related to the electron temperature T_e such as [32, 34]

$$D_e = \mu_e(k_b/e_0)T_e = \mu_e(k_b/e_0)(T_e/T)T, \tag{A.3}$$

where e_0 and T are the electron charge $(= 1.6 \times 10^{-19}\,\text{C})$ and the gas temperature (=298 K at NTP), respectively. The temperature ratio T_e/T is expressed as

$$T_e/T = 11.09 + 3.08\ln(E/P)$$
$$\text{for } E/P < 0.7\,\text{V cm}^{-1}\,\text{Torr}^{-1},$$
$$T_e/T = 15.36 + 14.9\ln(E/P)$$
$$\text{for } E/P \geqslant 0.7\,V\,\text{cm}^{-1}\,\text{Torr}^{-1},$$

where P is the pressure in Torr and E is the electric field in V cm^{-1}.

Electrical mobility of nanoparticles. The electrical mobility μ_d is given by [35]

$$\mu_d = \frac{e_0 C_c}{3\pi \eta_{vis} d}, \tag{A.4}$$

where η_{vis} and C_c are the dynamic viscosity of the carrier gas and the Cunningham slip correction factor, respectively.

Diffusion coefficient of nanoparticles. The diffusion coefficient D_d is given by the Stokes–Einstein relation [36]:

$$D_d = \frac{\mu_d k_b T}{e}, \tag{A.5}$$

where k_b and T are Bolzmann's constant and the translational temperature, respectively.

Attachment rate coefficient of ions-electrons to nanoparticles. The attachment coefficients $\beta^+_{d,q}$ and $\beta^-_{d,q}$ related to the interaction between an air ion onto a nanoparticle of diameter d with q elementary charges are given by Fuchs' model [2, 4] and are repeated as follows for completeness:

$$\beta^{\pm}_{d,q} = \pi \theta_{\pm} \gamma_{\pm} \bar{c}_{\pm} \delta^2_{\pm} \exp\left[-\frac{\Phi_{d,q}(\delta_{\pm})}{k_b T}\right] \times \left\{1 + \exp\left[-\frac{\Phi_{d,q}(\delta_{\pm})}{k_b T}\right] \frac{\theta_{\pm}\gamma_{\pm}\bar{c}_{\pm}\delta^2_{\pm}}{4a D_{\pm}} \times \int_0^{a/\delta_{\pm}} dy \exp\left[\frac{\Phi_{d,q}(a/y)}{k_b T}\right]\right\}^{-1}, \tag{A.6}$$

where y is a dimensionless integration variable ranging from 0 to $a/\delta_{\pm}$ with $a(= d/2)$ as the radius of the nanoparticles. The term $\Phi_{d,q}(r)$ corresponds to the electrostatic potential energy interaction:

$$\Phi_{d,q}(l) = \frac{e^2}{4\pi\varepsilon_0}\left[\frac{q}{l} - \frac{\varepsilon_r - 1}{\varepsilon_r + 1}\frac{a^3}{2l^2(l^2 - a^2)}\right], \tag{A.7}$$

which reflects the superposition of the Coulomb and image forces; l and ε_r are the interaction distance from the centre of the nanoparticle and the dielectric constant of them respectively. The mean thermal velocity $\bar{c}_{\pm}$ and the diffusion coefficient of air ions $D_{\pm}$ is given, respectively, by [37]

$$\bar{c}_{\pm} = \left(\frac{8k_b T}{\pi m_{\pm}}\right)^{1/2} \tag{A.8}$$

and

$$D_{\pm} = \frac{\mu_{\pm} k_b T}{e_0}, \tag{A.9}$$

where $m_{\pm}$ is the mass of the corresponding air ion in interaction with the nanoparticle.

The term $\delta_{\pm}$ corresponds to the radius of a limiting-sphere around the nanoparticle centre in which the air ions can be captured such as [38]

$$\delta_{\pm} = \frac{a}{Kn^2_{\pm}}\left[\frac{(1 + Kn_{\pm})^5}{5} - \frac{(1 + Kn^2_{\pm})(1 + Kn_{\pm})^3}{3} + \frac{2(1 + Kn^2_{\pm})^{5/2}}{15}\right], \tag{A.10}$$

where $Kn_{\pm}(= \lambda_{\pm}/a)$ is the air ion Knudsen number. The air ion mean free path is determined from Maxwell–Chapman–Enskog theory [39]:

$$\lambda_{\pm} = \frac{16\sqrt{2}}{3\pi(1 + \varepsilon)}\frac{D_{\pm}}{\bar{c}_{\pm}}\left(\frac{m_a}{m_a + m_{\pm}}\right)^{1/2}, \tag{A.11}$$

where m_a is the mass of neutral air molecules and $\varepsilon(= 0.132)$ is the correction factor when the colliding partners is assumed to be a hard sphere of unequal mass.

The term $\theta_{\pm}(= b^2/\delta^2_{\pm})$ describes the increase in collision of the air ions with the nanoparticle due to the presence of interaction forces by means of the impact parameter b. In the absence of electrical force, this impact parameter is equal to the radius of the nanoparticle ($b = a$). However, for the case of charged nanoparticles it is equal to the minimum distance b_{min} of the impact parameter which is given by the following relation [40]:

$$b^2 = l^2\left\{1 + \frac{2}{3k_b T}\left[\Phi_{d,q}(\delta_{\pm}) - \Phi_{d,q}(l)\right]\right\}. \tag{A.12}$$

The term $\gamma_{\pm}$ in equation (A.6) corresponds to the probability that an air ion which approaches within the distance $\delta_{\pm}$ is captured by the nanoparticle [41].

The attachment rate coefficients $\beta^e_{d,q}$ related to the interaction between an electron and a nanoparticle are similar to those of air ions. Indeed, the ionic terms $\theta_{\pm}$, $\gamma_{\pm}$, $\bar{c}_{\pm}$, $\delta_{\pm}$, $D_{\pm}$ and T in equation (A.6) are just substituted by those of electrons θ_e, γ_e, $\bar{c}_e$, δ_e, D_e and T_e, respectively:

$$\beta^e_{d,q} = \pi \theta_e \gamma_e \bar{c}_e \delta^2_e \exp\left[-\frac{\Phi_{d,q}(\delta_e)}{k_b T}\right] \times \left\{1 + \exp\left[-\frac{\Phi_{d,q}(\delta_e)}{k_b T}\right] \frac{\theta_e\gamma_e\bar{c}_e\delta^2_e}{4a D_e} \times \int_0^{a/\delta_e} dy \exp\left[\frac{\Phi_{d,q}(a/y)}{k_b T}\right]\right\}^{-1} \tag{A.13}$$

The diffusion coefficient for electrons D_e is given by equation (A.3), while the mean thermal velocity of electrons is expressed as [42, 43]:

$$\bar{c}_e = \left(\frac{2\, e_0\, D_e}{m_e \mu_e}\right)^{1/2}. \tag{A.14}$$

This can be used to define electron temperature and mean free path, respectively, as

$$T_e = \frac{m_e \bar{c}^2_e}{3k_b} \tag{A.15}$$

and

$$\lambda_e = \frac{m_e \bar{c}_e \mu_e}{e_0}. \tag{A.16}$$

The limiting-sphere radius δ_e related to electrons is obtained by substituting the electron mean free path, equation (A.15),

into equation (A.10), where the air ion Knudsen number is replaced by the electron Knudsen number $Kn_e(=\lambda_e/a)$:

$$\delta_e = \frac{a}{Kn_e^2}\left[\frac{(1+Kn_e)^5}{5} - \frac{(1+Kn_e^2)(1+Kn_e)^3}{3} + \frac{2(1+Kn_e^2)^{5/2}}{15}\right]. \quad \text{(A.17)}$$

Further, by substituting the limiting-sphere radius with the electron temperature into equation (A.12), one can obtain the term θ_e $(= b^2/\delta_e^2)$.

The diffusion theory (Fuchs' model) is used without explicitly designating the probability $\gamma_\pm$ that an ion is captured by a nanoparticle inside its limiting-sphere [3, 4], which leads implicitly to consider this probability to have a value equal to unity ($\gamma_\pm = 1$). However, the probability γ_e that an electron is captured by a nanoparticle inside its limiting-sphere is found to have a value lower than unity [6]. Note that Romay [42] also found values lower than unity for the capture probability of an electron (called accommodation coefficient) by calculating attachment rate coefficients between an uncharged nanoparticle and an electron with helium and nitrogen gas carrier.

References

[1] Friedlander S K and Pui D Y H 2004 *J. Nanopart. Res.* **6** 313
[2] Fuchs N A 1963 *Geofis. Pura. Appl.* **56** 185
[3] Pui D Y H, Fruin S and McMurry P H 1988 *Aerosol Sci. Technol.* **8** 173
[4] Adachi M, Kousaka Y and Okuyama K 1985 *J. Aerosol Sci.* **16** 109
[5] Marquard A, Kasper M, Meyer J and Kasper G 2005 *J. Electrostast.* **63** 693
[6] Aliat A, Tsai C J, Hung C T and Wu J S 2008 *Appl. Phys. Lett.* **93** 154103
[7] Gallimberti I 1998 *J. Electrostat.* **43** 219
[8] Borra J P 2006 *J. Phys. D: Appl. Phys* **39** R19
[9] Dumitran L M, Dascalescu L, Atten P and Notingher P V 2006 *IEEE Trans. Indust. Appl.* **42** 378
[10] Dumitran L M, Dascalescu L, Notingher P and Atten P 2007 *J. Electrostat.* **65** 758
[11] Khaddour B, Atten P and Coulomb J L 2008 *J. Electrostat.* **66** 254
[12] Goldman M and Goldman A 1978 *Corona Discharges Gaseous Electronics* I vol 89b, ed M N Hirsh 119pp
[13] Chen J and Davidson J H 2002 *Plasma Chem. Plasma Process.* **22** 199
[14] Batina J, Noel F, Lachaud S, Peyrous R and Loiseau J F 2001 *J. Phys. D: Appl. Phys.* **34** 1510
[15] Soria C, Pontiga F and Castellanos A 2004 *Plasma Sources Sci. Technol.* **13** 95
[16] Yanallah K, Hadj Ziane S, Belasri A and Meslem Y 2006 *J. Mol. Struct-Theochem* **777** 125
[17] Deutsch W 1933 *Ann Phys.* **5** 588
[18] Oussalah N and Zebboudj Y 2006 *Eng. Comput.* **21** 296
[19] Kaptzov N A 1947 *Elektrischeskiye Yavleniya v Gazakh i Vacuume* (Moscow: OGIZ)
[20] Peek F W 1929 *Dielectric Phenomena in High-Voltage Engineering* (New York: McGraw-Hill)
[21] Morrow R 1997 *J.Phys. D: Appl. Phys.* **30** 3099
[22] Pontiga F, Soria C, Castellanos A and Skalny J D 2002 *Ozone Sci. Eng.* **24** 447
[23] Takahashi Y, Yoshida M, Anma Y, Kobayashi S and Endo M 1982 *J. Phys. D: Appl. Phys.* **15** 639
[24] Conwell E M 1953 *Phys. Rev.* **90** 769
[25] Dumitran L M, Atten P and Blanchard D 2004 *Inst. Phys. Conf. Ser.* vol 178 (Bristol: Institute of Physics Publishing) pp 199–205
[26] Turner J H, Lawless P A, Yamamoto T and Coy D W 1995 Electrostatic Precipitators *Air Pollution Engineering Manual* ed W T Davis (New York: Wiley) chapter 6, http://p2pays.org/ref/10/09854.pdf
[27] Parker K R 1997 *Applied Electrostatic Precipitation* (London: Blackie)
[28] Arkadi Maisels, Jordan F, Kruis F E and Fissan H 2003 *J. Nano-part. Res.* **5** 225
[29] Borra J P 2008 *Plasma Phys. Control. Fusion* **50** 124036
[30] Alguacil F J and Alonso M 2006 *J. Aerosol Sci.* **37** 875
[31] Zanoun E S, Durst F, Bayoumy O and Al-Salaymeh A 2007 *Exp. Therm. Fluid Sci.* **32** 249
[32] Abdel-Salam M, Nakamo M and Mizumo A 2007 *J. Phys. D: Appl. Phys.* **40** 1919
[33] Badaloni B and Gallimberti I 1972 *Basic Data of Air Discharges* (Padua, Italy: Università di Padova)
[34] Brown S C 1959 *Basic Data of Plasma Physics* (Cambridge, MA: Technology Press of MIT)
[35] Hinds W C 1998 *Aerosol Technology* 2nd edn (New York: Wiley)
[36] Flower W L 1983 *Phys. Rev. Lett.* **51** 2287
[37] Jiang J, Lee M H and Biswas P 2007 *J. Electrostast.* **65** 209
[38] Write P G 1960 *Faraday Discuss.* **30** 100
[39] Bricard J 1965 *Problems of Atmospheric and Space Electricity* (Amsterdam: Elsevier) 82pp
[40] Natanson G L 1960 *Sov. Phys.—Tech. Phys.* **5** 538
[41] Rapp M 2000 *J. Aerosol Sci.* **31** 1367
[42] Romay F J 1992 *PhD Thesis* University of Minnesota, Minneapolis, MN
[43] Dutton J 1975 *J. Phys. Chem. Ref. Data.* **4** 577